

Effects of exhaust gas recirculation in diesel engines featuring late PCCI type combustion strategies

Original

Effects of exhaust gas recirculation in diesel engines featuring late PCCI type combustion strategies / D'Ambrosio, Stefano; Ferrari, Alessandro. - In: ENERGY CONVERSION AND MANAGEMENT. - ISSN 0196-8904. - 105:(2015), pp. 1269-1280. [10.1016/j.enconman.2015.08.001]

Availability:

This version is available at: 11583/2628090 since: 2016-01-13T17:09:54Z

Publisher:

Elsevier Ltd

Published

DOI:10.1016/j.enconman.2015.08.001

Terms of use:

This article is made available under terms and conditions as specified in the corresponding bibliographic description in the repository

Publisher copyright

Elsevier postprint/Author's Accepted Manuscript

© 2015. This manuscript version is made available under the CC-BY-NC-ND 4.0 license
<http://creativecommons.org/licenses/by-nc-nd/4.0/>. The final authenticated version is available online at:
<http://dx.doi.org/10.1016/j.enconman.2015.08.001>

(Article begins on next page)

1 **EFFECTS OF EXHAUST GAS RECIRCULATION IN DIESEL ENGINES FEATURING**
2 **LATE PCCI TYPE COMBUSTION STRATEGIES**

3 *d'Ambrosio, S*, and Ferrari, A.*

4 *Energy Department – Politecnico di Torino*

5 *C.so duca degli Abruzzi, 24, 10129, Torino, Italy.*

6 **1. ABSTRACT**

7 The influence of exhaust gas recirculation (*EGR*) has been analyzed considering experimental results obtained from a
8 Euro 5 diesel engine calibrated with an optimized pilot-main double injection strategy. The engine features a late
9 premixed charge compression ignition (*PCCI*) type combustion mode and different steady-state key-points that are
10 representative of the engine application in a passenger car over the New European Driving Cycle (*NEDC*) have been
11 studied. The engine was fully instrumented to obtain a complete overview of the most important variables. The pressure
12 time history in the combustion chamber has been measured to perform calculations with single and three-zone
13 combustion diagnostic models. These models allow the in-cylinder emissions and the temperature of the burned and
14 unburned zones to be evaluated as functions of the crankshaft angle.

15 The *EGR* mass fraction was experimentally varied within the 0÷50% range. The results of the investigation have shown
16 the influence that high *EGR* rates can have on intake and exhaust temperatures, in-cylinder pressure and heat release
17 rate time histories, engine-out emissions (*CO*, *HC*, *NO_x*, soot), brake specific fuel consumption and combustion noise
18 for a *PCCI* type combustion strategy. The outputs of the diagnostic models have been used to conduct a detailed
19 analysis of the cause-and-effect relationships between the *EGR* rate variations and the engine performance. Finally, the
20 effect of the *EGR* on the cycle-to-cycle variability of the engine torque has been experimentally investigated.

21 **Keywords:** exhaust gas recirculation; pollutant emissions; partial *PCCI* diesel engines.

22 **Highlights:**

- 23 - The effects that a high *EGR* rate can have on *PCCI* type combustion strategies have been analyzed.
24 - The dependence of engine emission and combustion noise on *EGR* has been addressed.

* Corresponding author e-mail address: stefano.dambrosio@polito.it

25 - The time histories of the main in-cylinder variables have been plotted for different *EGR* rates.

26 **2. INTRODUCTION.**

27 Conventional diesel engines are lean burning systems, if the overall air-fuel ratios are considered [1]. A premixed
28 combustion phase is followed by a mixing-controlled combustion stage, in which the oxidation reactions are much
29 faster than the diffusion rate of the fuel in the charge [2, 3]. Most of the fuel burns in the diffusion controlled phase and
30 the flames are located at approximately stoichiometric regions within the overall lean, but locally inhomogeneous
31 mixture. As a consequence, high flame temperatures, which can be estimated through adiabatic stoichiometric
32 temperature calculations [4, 5], are obtained in the presence of oxygen and nitrogen and large amounts of NO_x are
33 therefore generated [6, 7]. Diffusive combustion is also responsible for most of the soot generation [2] because of the
34 presence of rich pockets within the cylinder, which cannot find the necessary oxygen amount during the later stages of
35 combustion, especially when the engine is working at high loads [1].

36 External exhaust gas recirculation (*EGR*) is a strategy that is adopted in diesel engines to reduce combustion flame
37 temperatures, which are responsible for high NO_x formation. The result of *EGR* utilization is that most of the elemental
38 nitrogen is emitted as harmless N_2 [8-13]. Furthermore, *EGR* also has a positive effect on engine noise because it limits
39 the heat release rate (*HRR*) during premixed combustion, which is usually characterized by rapid burning fuel [14].
40 However, the application of the *EGR* can determine penalties in terms of engine emissions and performance, such as
41 particulate matter (*PM*), *CO*, unburned hydrocarbons (*HC*) and a deterioration in the brake specific fuel consumption
42 (*bsfc*) [15-18]. In particular, extremely high values of *EGR* negatively affect the diffusive combustion process, as they
43 increase the soot emissions and induce a rise in the cycle-to-cycle variability of combustion [1]. Nevertheless, the
44 increase in soot generation for increasing *EGR* rates determines higher radiation and a consequent decrease in the flame
45 temperatures that can help to further diminish NO_x emissions [8]. Finally, *EGR* can adversely affect the quality of the
46 lubricating oil and engine durability because of increased wear between the piston rings and the cylinder liner [11, 19-
47 21].

48 The benefits, with respect to the NO_x emissions, depend on the various effects-induced by *EGR*: a dilution effect, a
49 thermal effect and a chemical effect [8, 13, 22, 23]. The dilution effect of *EGR* involves a decrease in the in-cylinder
50 oxygen concentration of the inducted charge with the main consequence of decelerating the mixing process between the
51 injected fuel and oxygen. In addition, the quantity of inert gas that can absorb the heat release increases, and this gives
52 rise to lower flame temperatures.

53 The thermal effect consists of an increase in the heat capacity of the inducted charge, because of the augmented average
54 specific heat of the exhaust gas, which contains large amounts of CO_2 and H_2O , i.e. triatomic gases, compared to fresh

55 air, which mainly contains O_2 and N_2 , i.e. diatomic gases. The CO_2 and H_2O concentrations in the exhaust gas are low at
56 part loads, due to an overall leaner mixture, and, as a result, *EGR* is more effective at high loads [4, 11]. As a
57 consequence, high *EGR* levels are required to drastically reduce the NO_x emissions at low loads [9]. Another effect,
58 which should be included in the thermal effect of *EGR*, is due to the increase in the inlet temperature of the charge as
59 the *EGR* rate is augmented, since the exhaust gas temperature is higher than that of fresh air. Therefore, a reduction in
60 the charge density and in the in-cylinder trapped mass is obtained as the *EGR* rate grows under constant boost pressure.
61 This behavior is referred to as thermal throttling [2, 8] and it determines a negative effect on NO_x reduction, since it
62 tends to increase the maximum temperature of the burned gas, because of the higher temperature of the induced charge
63 and roughly the same energy of the fuel absorbed by a smaller in-cylinder mass. The negative effect of thermal
64 throttling can prevail over the beneficial thermal effect of the increased specific heat [24] in the final determination of
65 the maximum burned gas temperature. Therefore, the utilization of cooled *EGR* is recommended [6, 25] in order to
66 mitigate the negative effect of thermal throttling (if the cooled *EGR* temperature were the same as that of the fresh air,
67 thermal throttling would not be present) and thus to limit the maximum in-cylinder temperature of the burned gas. The
68 benefits of the cooled *EGR* strategy augment at high *EGR* rates, and advantages can also be observed in terms of *bsfc*
69 and soot control [12].

70 The third main effect of *EGR* is of chemical nature and is due to the CO_2 and H_2O species that are present in the exhaust
71 gas and which tend to dissociate during combustion, thus reducing the peak combustion temperature and contributing to
72 the inhibition of NO_x formation.

73 When the *EGR* strategy is applied to a diesel engine, the three previously mentioned effects are present simultaneously.
74 If a part of the oxygen content is replaced by *EGR* in the cylinder, the given amount of injected fuel has to diffuse over
75 a wider volume before a sufficient stoichiometric mixture can be formed. The thus obtained larger stoichiometric region
76 contains additional quantities of CO_2 , H_2O and N_2 , which can absorb part of the combustion-released energy and
77 undergo dissociation phenomena, which lead to even lower flame temperatures [10, 22].

78 Several experiments have been performed with the purpose of evaluating the individual impact of the three
79 abovementioned effects [8, 22]. The dilution effect is responsible for most of the NO_x reduction, and the second effect,
80 in terms of potential, is the chemical one, while the thermal effect is generally the least important [24, 2].

81 As far as the influence of *EGR* on the fuel ignition delay is concerned [26, 27], the drop in the oxygen concentration,
82 due to the dilution effect, slows down the auto-ignition reactions and enlarges the ignition delay, whereas the thermal
83 throttling effect exerts an opposite influence [8], due to the abovementioned temperature increase of the induced charge.

84 The dilution effect generally prevails over thermal throttling and the ignition delay therefore usually increases with the

85 *EGR* rate and allows more fuel to be evaporated and mixed with the air before combustion starts: the final result is an
86 intensified premixed combustion mode [26].

87 New engine concepts related to low-temperature combustion (*LTC*), such as homogeneous charge compression ignition
88 (*HCCI*) and partial premixed charge compression ignition (*PCCI*), are based on the utilization of large amounts of *EGR*
89 in order to obtain a remarkable reduction in both NO_x and *PM* engine out emissions without aftertreatment systems [28],
90 which require space, additional costs and complexities [29]. High *EGR* rates reduce peak burned gas temperatures and
91 prolong the ignition delay, thus promoting the dispersion of the injected fuel in the charge in order to obtain highly
92 premixed combustion. The engine *bsfc* also improves in the *LTC*, due to almost instantaneous combustion. Although
93 *LTC* is a highly promising strategy, it is still difficult to control the combustion and to extend the strategy to the medium
94 and high-load range of the engine [30, 31]. Furthermore, the *HC* and *CO* emissions at low engine loads represent a
95 major concern for the low temperature combustion typology [32, 33]. In fact, the quantity of supplied fuel at light loads
96 is small and oxidation reactions are quite slow, due to the very lean mixture and low temperatures [34]. The ignition
97 delay is extended and this leads to increased over-mixed areas that are outside the fuel flammability limits [33].
98 Furthermore, retarded main injection timings, which are typical of late *PCCI* combustion strategies, further decrease
99 peak in-cylinder temperatures. Over-mixing and bulk quenching mechanisms are considered the dominant causes of the
100 increased *HC* and *CO* emissions in *PCCI* engines. In addition, impingement can also occur in engines managed with
101 early *PCCI* combustion modes.

102 The practical implementation of the *EGR* strategy is straightforward for naturally aspirated diesel engines, because the
103 backpressure in the exhaust tailpipe is normally higher than the intake pressure [1]. A long-route (or low-pressure) *EGR*
104 loop [35] can be applied to turbocharged diesel engines, since a positive differential pressure is generally available
105 between the turbine outlet and the compressor inlet. However, conventional compressors and intercoolers are not
106 designed to endure diesel exhaust gas temperatures and high fouling levels. Therefore, the preferred solution would be
107 to recycle the exhaust gas from upstream of the turbine to downstream of the compressor in the intake manifold, i.e. a
108 short-route (or high-pressure) *EGR* loop would be adopted. However, this *EGR* layout is only applicable when the
109 upstream pressure of the turbine is sufficiently higher than the boost pressure [1]. An efficient exploitation of the
110 exhaust gas can be obtained by adopting a variable geometry turbine that can effectively provide the desired pressure
111 level upstream of the turbine [23, 25]. In these systems, the *EGR* control is closely related to the variable geometry
112 turbine control [36]. A very high *EGR* rate leads to an appreciable decrease in the gas flow through the turbine, and
113 hence to a possible consequent decrease in boost pressure. For this reason, it is not feasible that a considerable reduction
114 in NO_x could be achieved without any penalties on soot emissions for most short-route *EGR* layouts. Possible

115 improvements could be obtained by applying twin-stage turbocharger setups or by combining high-pressure and low-
116 pressure *EGR* layouts [8].

117 The present work explores the influence of cooled *EGR* mass fractions for values of up to around 50% for a Euro 5 low
118 compression ratio diesel engine, equipped with a twin-stage turbocharger and run on a late *PCCI* type combustion
119 strategy. Even though the *EGR* strategy has been studied extensively in conventional diesel engines with up to 30-40%
120 *EGR* rates [35, 37], a great deal of attention is still being paid to the effects of multiple injections in the presence of
121 heavy *EGR* rates [38, 39], which are typical of *LTC* applications. *EGR* trade-offs have been performed under different
122 steady-state working conditions that correspond to the installation of the engine on a *D*-segment vehicle that runs the
123 European emission homologation cycle. The investigation was based on experimental results obtained at the test bench.
124 Furthermore, simulations were performed using one- and three-zone combustion diagnostic models to investigate the
125 cause-and-effect relationships of the physical events.

126 **3. EXPERIMENTAL SET-UP.**

127 The experimental tests have been carried out on the highly-dynamic test bed installed at the Politecnico di Torino
128 ICEAL (IC Engines Advanced Laboratory). The test bench was equipped with an ‘ELIN AVL APA 100’ cradle-
129 mounted AC dynamometer, while an ‘AVL KMA 4000’ with a reading accuracy of 0.1% over a 0.28-110 kg/h range
130 was used to continuously meter the fuel consumption. Furthermore, an ‘AVL AMAi60’ system, made up of three
131 analyzer trains, was utilized to measure the raw engine-out gaseous emissions. Two analyzer trains were equipped with
132 devices for the analysis of the *HC*, *CH₄*, *NO_x*, *CO*, *CO₂* and *O₂* species. The third analyzer train included a detector,
133 which was used to measure the *CO₂* levels in the intake manifold, in order to evaluate the *EGR* rate. Finally, an AVL
134 415S smokemeter allowed the soot emissions in the exhaust gases to be evaluated.

135 The test engine was fully instrumented with piezoresistive pressure transducers and thermocouples in order to measure
136 the pressure and temperature in the intake, exhaust and *EGR* lines of the engine. A high-frequency piezoelectric
137 transducer was installed in the glow-plug seat to measure the pressure time-history of the gases in the combustion
138 chamber of one cylinder and one of the piezoresistive transducers was used to detect the pressure level in the inlet
139 runner of the same cylinder and thus to reference the in-cylinder pressure. All of the abovementioned measurement
140 devices are controlled by the PUMA OPEN 1.3.2 and the Indicom 1.6 automation systems.

141 The engine, whose main features are reported in Table 1, features a low compression ratio (16.3:1), which is in line with
 142 typical *PCCI* applications. The twin-stage turbocharger is controlled by means of two waste-gate valves. The short-
 143 route *EGR* system includes a cooled *EGR* valve on the exhaust side, which is controlled on the basis of the airflow
 144 feedback signal; a shell and tube type *EGR* cooler is placed before this valve. Furthermore, a throttle valve assembly has
 145 been placed in the intake system, downstream of the engine intercooler and just upstream of the junction with the *EGR*
 146 gases. The use of intake throttling increases the pressure drop in the *EGR* loop, and thus allows the *EGR* rate to be
 147 increased at low loads.

| | |
|---------------------------|--|
| Engine type | 2.0L Euro 5 |
| Displacement | 1956 cm ³ |
| Bore x stroke | 83.0 mm x 90.4 mm |
| Compression ratio | 16.3 |
| Valves per cylinder | 4 |
| Turbocharger | Twin-stage with valve actuators and waste-gate |
| Fuel injection system | Common Rail 2000 bar piezo |
| Specific power and torque | 71 kW/l – 205 Nm/l |

Table 1: Main specifications of the reference engine.

| Key-point | SOI _{Pil} (°bTDC) | q _{Pil} (mm ³ /cyl) | SOI _{Main} (° bTDC) |
|-----------|-------------------------------|--|---------------------------------|
| 1500×2 | 11 | 1.7 | -2 |
| 1500×5 | 12 | 1.6 | -1 |
| 2000×2 | 16 | 1.5 | -1 |
| 2000×5 | 17 | 1.4 | 0 |
| 2500×8 | 25 | 1.2 | 4 |
| 2750×12 | 31 | 1.1 | 7 |

Table 2: ECU parameters for the different key-points.

148 The engine was preliminarily calibrated by applying an optimized pilot-main double injection strategy, which in the
 149 present work is referred to as the baseline calibration. Steady-state tests were performed at some engine key-points,
 150 which were considered representative of the engine application to a *D*-segment passenger car over the new European
 151 driving cycle (*NEDC*). The considered key-points were expressed in terms of n (rpm) \times b_{mep} (bar) as follows: 1500×2,
 152 1500×5, 2000×2, 2000×5, 2500×8, 2750×12.

153 Table 2 reports the values of the pilot injection fuel quantity per cycle and per cylinder (q_{Pil}) as well as the injection
 154 timing for both the pilot (SOI_{Pil}) and main (SOI_{Main}) injection pulses. Negative values of SOI_{Main} mean that the injection
 155 occurred after the *TDC*. The quantity of the main injection was set automatically by the test bench control system in
 156 order to maintain the desired b_{mep} value. As can be inferred, the main injection timing is delayed at low loads and the
 157 pilot-to-main injection dwell times are long, in line with late *PCCI* strategies.

158 *EGR* trade-off curves were carried out at each key-point in the neighborhood of the baseline calibration point by
 159 varying the quantity of inducted air-per-cylinder and stroke, while keeping all the other engine parameters fixed.

160 The *EGR* mass fraction is defined as the ratio of the recirculated exhaust gas mass flow-rate to the total mass flow-rate
 161 that is inducted in the cylinder [9, 12]:

162

$$X_{EGR} = \frac{\dot{m}_{EGR}}{\dot{m}_{EGR} + \dot{m}_a} \quad (1)$$

163

where \dot{m}_{EGR} and \dot{m}_a are the *EGR* and fresh-air mass flow-rates, respectively. In the present investigation the calculation

164

of X_{EGR} was performed considering the accurate expression developed in [40], which requires the evaluation of the

165

volume concentrations of all the species at the engine exhaust and knowledge of the combustion air composition at the

166

engine inlet. The *EGR* mass fraction can also be estimated by CO_2 volume concentration measurements in the intake

167

manifold $[CO_2]_{int}$, and at the engine exhaust $[CO_2]_{exh}$ according to the following simplified formula, where $[CO_2]_{amb}$

168

represents the CO_2 volume concentration in the external environment:

169

$$X_{EGR} = \frac{[CO_2]_{int} - [CO_2]_{amb}}{[CO_2]_{exh} - [CO_2]_{amb}} \quad (2)$$

170

4. STEADY-STATE TESTS.

171

The *EGR* trade-off curves are plotted for the different key-points with distinct symbols, which are reported in the legend

172

of each graph. The baseline calibration points are highlighted in each diagram with a thin line that contours the

173

corresponding symbol.

174

The global air-fuel ratio, λ , is reported in Fig. 1 as a function of X_{EGR} for the different key-points. It can be observed

175

that, for the baseline calibration key-points, the lower the load, the higher the adopted *EGR* rate: $X_{EGR} \approx 45 \div 50\%$ at the

176

lowest load ($bmeP = 2$ bar), $X_{EGR} \approx 30 \div 35\%$ at medium load ($bmeP = 5$ bar) and $X_{EGR} \approx 20 \div 25\%$ at the highest loads ($bmeP$

177

$= 8$ and $bmeP = 12$ bar). These values are higher than those usually applied in conventional diesel engines [35, 37].

178

The application of *EGR* limits the volume available for fresh air within the cylinder. The λ variable is generally shown

179

to decrease almost linearly with X_{EGR} for any key-point, because the quantity of fuel is almost independent of the *EGR*

180

mass fraction at fixed load [12]. A deviation of the λ - X_{EGR} curve from linearity can be noticed for the highest values of

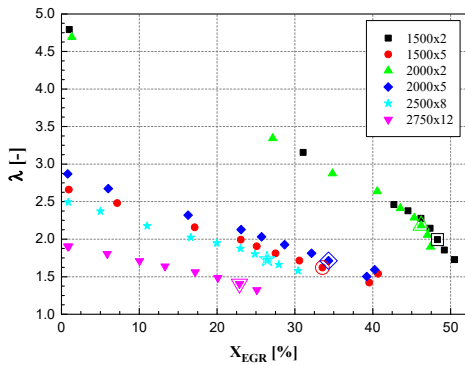


Figure 1. Relative air-fuel ratio λ versus X_{EGR}

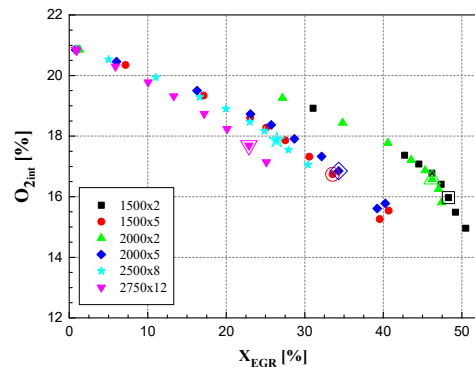


Figure 2. Oxygen volume concentration versus X_{EGR} .

181 X_{EGR} . In these conditions, a high mass flow-rate of gases is sent back from the engine exhaust to the intake manifold,
 182 bypassing the turbine, whereas the fresh-air flow is decreased using the intake throttle valve. As a consequence, it is not
 183 possible to maintain the desired level of boost pressure (p_{int}), which is set by the *ECU*, in the intake manifold for
 184 $X_{EGR} \geq 40\%$, due to both the insufficient enthalpy flux of the exhaust gases entering the turbine and to air throttling,
 185 which reduces the pressure level in the manifold. Therefore, both the air mass flow-rate and λ decrease more than
 186 proportionally with the *EGR* mass fraction for $X_{EGR} \geq 40\%$.

187 Figure 2 shows that an increase in X_{EGR} has a great impact on the dilution effect, because it can reduce the oxygen
 188 volume concentration $[O_2]_{int}$ in the intake manifold to a great extent, compared to the value of around 21%, which
 189 corresponds to the oxygen concentration in environmental air. In particular, *EGR* is more effective at high loads than at
 190 low loads, because the same $[O_2]_{int}$ can be obtained with a smaller X_{EGR} . In fact, as already mentioned, the CO_2 and H_2O
 191 concentrations in the exhaust gas are lower at lighter loads, since the concentrations of these species increase with the
 192 equivalence ratio $\phi = 1/\lambda$. Therefore, relatively high *EGR* rates are required at low loads in order to obtain significant
 193 reductions in NO_x emissions. This explains why, the lower the load for the baseline calibration key-points in Fig. 1, the
 194 higher the X_{EGR} . In general, the load dependence of the $[O_2]_{int}$ reduction on X_{EGR} is significant, whereas the influence of
 195 the engine speed on the $[O_2]_{int}$ - X_{EGR} curves is negligible.

196 The inlet temperature of the in-cylinder charge also rises with the *EGR* rate (Fig. 3). This produces a thermal throttling
 197 effect that occurs because the *EGR* cooler is not able to cool the recirculated exhaust gas to the same temperature as the
 198 air downstream of the intercooler. The higher the load or the speed, the higher the temperature of the gases at the engine
 199 exhaust and the higher the T_{int} temperature for a given X_{EGR} value. Thermal throttling is also induced by the increased
 200 internal residual gas fraction (internal *EGR*) that results from the growth of the exhaust manifold pressure as X_{EGR}
 201 increases. In particular, the pressure difference between the exhaust manifold and the intake manifold, which is
 202 responsible for the internal *EGR*, grows significantly for $X_{EGR} \geq 40\%$, because of the intake throttle valve action.

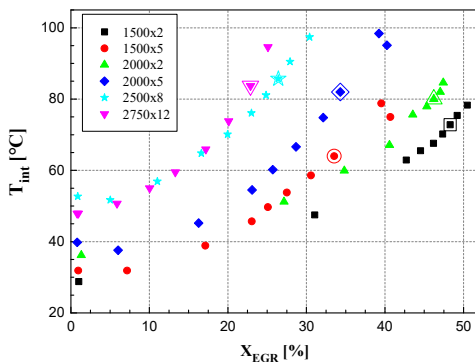


Figure 3. Engine inlet temperature versus X_{EGR} .

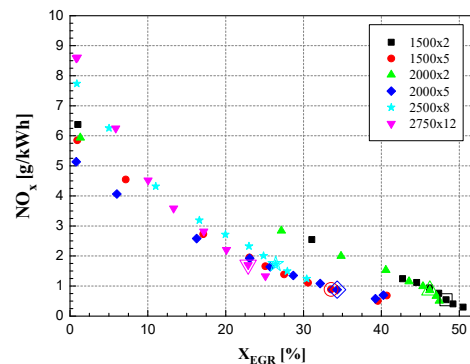


Figure 4. NO_x emissions versus X_{EGR} .

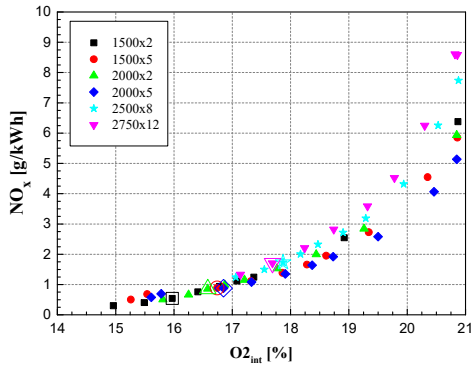


Figure 5. NO_x emissions versus O_2 .

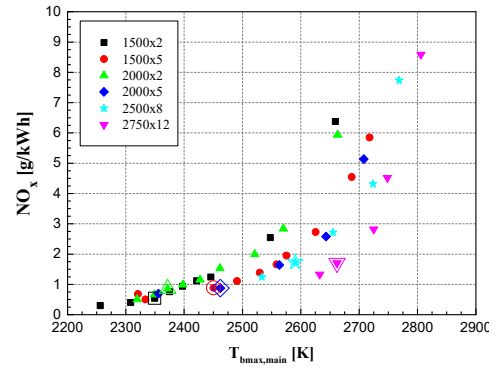


Figure 6. NO_x emissions versus $T_{bmax,main}$.

203 Figures 4 and 5 show the dependence of the specific NO_x emissions on the EGR rate and on the corresponding oxygen
 204 volume concentration in the intake manifold, respectively. Dilution is the effect that has most influence on the
 205 remarkable reduction in NO_x , as the X_{EGR} increase determines the $[O_2]_{int}$ diminution that can be observed in Fig. 5.
 206 Results, which are in agreement with those in Fig. 4, were obtained for conventional combustion mode diesel engines in
 207 [12, 18, 26] and in [27], where a reduction of approximately 50% was achieved in the NO_x emissions under $X_{EGR} \approx 20\%$
 208 for medium load and speed. A better defined trend, which is almost independent of the specific key-point, can be seen
 209 more easily in Fig. 5 than in Fig. 4.

210 The reduction in the NO_x species at $bmeP=2$ bar and $bmeP=5$ bar is also due to the retarded main injection timing
 211 (cf. SOI_{Main} in Table 2), which postpones the combustion well into the expansion stroke. In $PCCI$ type engines, retarded
 212 injection can be a complementary strategy to EGR for NO_x control, even though the former leads to increased fuel
 213 consumption and deteriorates HC emissions [11, 27].

214 In general, NO_x emissions are mainly affected by two factors: the presence of oxygen in the charge and the peak value
 215 of the burned-gas temperature [41]. EGR reduces both the oxygen volume concentration and the peak temperature of
 216 the burned gases. If the NO_x emissions are plotted as a function of the maximum burned gas temperature of the main
 217 shot (T_{bmax} has been calculated by means of a 3 zone combustion model [42]), instead of $[O_2]_{int}$, the pattern observed in
 218 Fig. 6 is achieved. However, the best correlation for NO_x is obtained with respect to $[O_2]_{int}$ in Fig. 5.

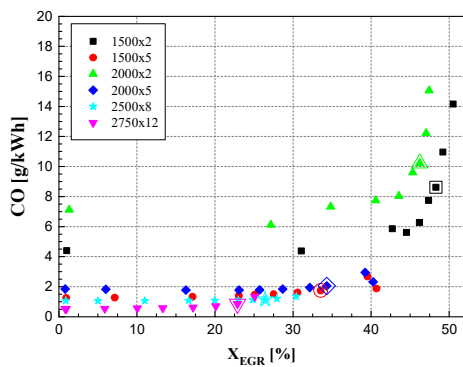


Figure 7. HC emissions versus X_{EGR} .

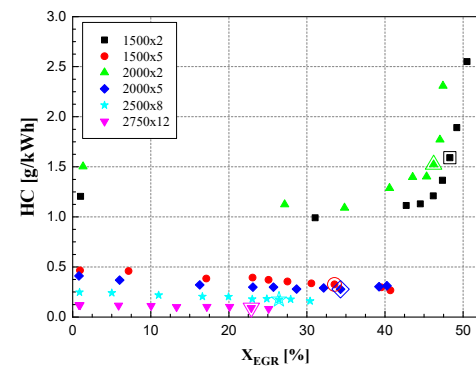


Figure 8. CO emissions versus X_{EGR} .

219 The minimum *EGR* rate that is sufficient to decrease the peak temperature of the burned gas below an acceptable
 220 threshold depends on the engine key-point and on the trade-off among different targets (i.e., the limits of different
 221 pollutant emissions set by regulations, fuel consumption and combustion noise), as well as on the synergy between
 222 combustion strategies and the aftertreatment devices installed in the exhaust pipe. The dilution, chemical and thermal
 223 effects of *EGR* simultaneously affect $T_{bmax,main}$ and it is a difficult task to properly split the contribution of each *EGR*
 224 effect during normal engine operation conditions because they occur at the same time. The calculations of the thermal
 225 properties of air and exhaust gases for the tests considered in the current investigation showed that the specific heat of
 226 the *EGR* could be up to 6% higher than the specific heat of the air, whereas the increase in the thermal capacity of the
 227 inlet charge was up to 2.5%. This variation is not able to account for the great temperature reduction in the maximum
 228 burned gas temperature that can be appreciated by considering both Figs. 4 and 6. Therefore, it can be stated that the
 229 dilution and chemical effects are more important than the thermal effect, a result that is in line with the findings in [2].
 230 The *CO* and *HC* emissions versus X_{EGR} are plotted in Figs. 7 and 8 and show similar trends, the *CO* emissions being
 231 roughly 5 times higher than the corresponding *HC* emissions. In general, *CO* and *HC* emissions reduce as the load
 232 increases. In particular, as soon as the combustion temperature exceeds 1400-1500 K, *CO* rapidly oxidizes to CO_2 [33,
 233 43]. The influence of the *EGR* rate on the *HC* and *CO* emissions is reduced for lower X_{EGR} values than 30%-40%, as can
 234 be seen in Figs. 7 and 8. Even the *HC* emissions exhibit a slightly decreasing trend for X_{EGR} up to 35-40% and this trend
 235 can be explained considering that the fuel can always find enough air to burn for low X_{EGR} values. As a consequence,
 236 the dilution effect of *EGR*, which impacts negatively on *HC* emissions, becomes negligible, while the thermal throttling
 237 effect of *EGR* (Fig. 3), which can promote *HC* oxidation, plays a decisive role. *HC* and *CO* emissions increase to a great
 238 extent for higher *EGR* mass fractions than 40%, as can be seen in Figs. 7 and 8, due to incomplete combustion. In fact,
 239 even though the global λ continues to be lean, the mixture is inhomogeneous and, locally, some fuel cannot find the
 240 necessary quantity of air. However, if the turbocharger can provide a sufficiently increased boost pressure, in order to

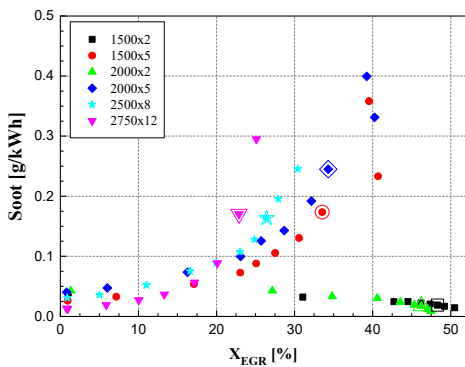


Figure 9. Soot emissions versus X_{EGR} .

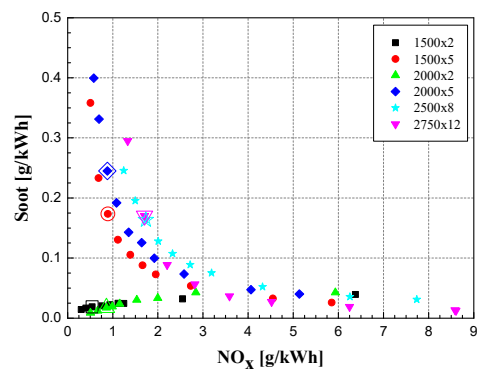


Figure 10. NO_x -soot curve as X_{EGR} varies.

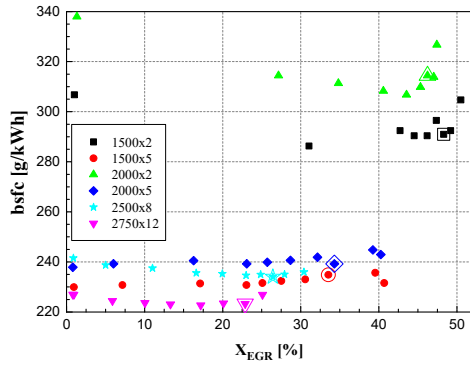


Figure 11. Brake specific fuel consumption versus X_{EGR} .

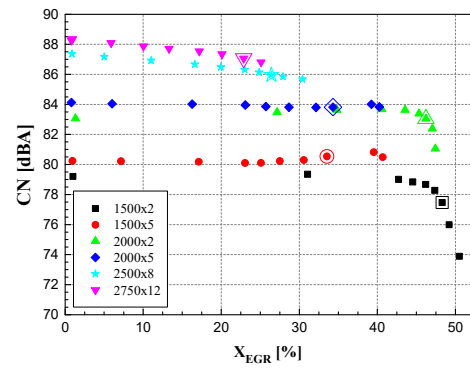


Figure 12. Combustion noise versus X_{EGR} .

241 maintain adequate local ϕ values, the combustion deterioration will practically be negligible. Therefore, almost similar
 242 reductions in NO_x as those shown in Fig. 5 would be achieved, but with minor increases in the CO and HC emissions.
 243 Soot emissions versus X_{EGR} are plotted in Fig. 9, where different trends, with respect to the EGR rate, can be observed
 244 on the basis of the considered load [15]. At the lowest loads ($bme_p = 2$ bar), the soot emissions decrease as X_{EGR}
 245 increases, but, when the load is increased, it is difficult to employ high EGR rates, due to the deterioration in diffusive
 246 combustion, which makes the engine generate more smoke. This sensitivity of soot to EGR at medium and high loads is
 247 consistent with the data in [39]. Therefore, a trade-off limit must be set for X_{EGR} at medium and high loads in order to
 248 obtain a suitable compromise between NO_x and soot emissions; from this point of view, a high injection pressure or
 249 swirl ratio can also be used to suppress soot and allow the EGR limit to be raised [38]. Fig. 10 reports the NO_x -soot
 250 trade off curves that are obtained for $bme_p = 5$ bar, $bme_p = 8$ bar and $bme_p = 12$ bar by varying X_{EGR} . An increase in
 251 X_{EGR} has a positive influence on both NO_x and soot emissions at $bme_p = 2$ bar, since the engine works in the $PCCI$
 252 regime. However, if the engine is not run under a $PCCI$ type strategy, the presence of the NO_x -soot EGR trade-off also
 253 persists at low loads [44]. This topic will be dealt with in more detail in section 5, where the in-cylinder analysis is
 254 presented.
 255 Figure 11 reports $bsfc$ as a function of X_{EGR} for different bme_p values. A decrease in $bsfc$ can be found when passing
 256 from no EGR to around $X_{EGR} \approx 30\%$ at $bme_p = 2$ bar. This is related to the combustion of the unburned hydrocarbons that
 257 enter the combustion chamber with the recirculated exhaust gas [11]. In fact, the exhaust gas contains more O_2 at bme_p
 258 $= 2$ bar than at higher loads. Furthermore, as already mentioned, cooled EGR acts as a pre-heater of the intake mixture.

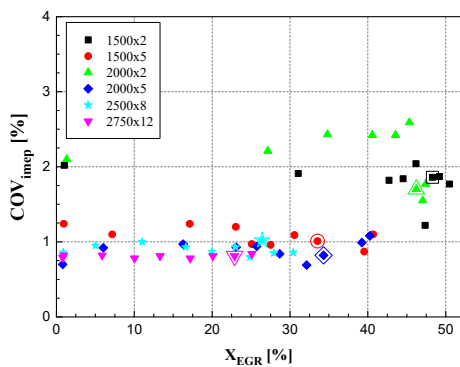


Figure 13. COV_{imep} versus X_{EGR} .

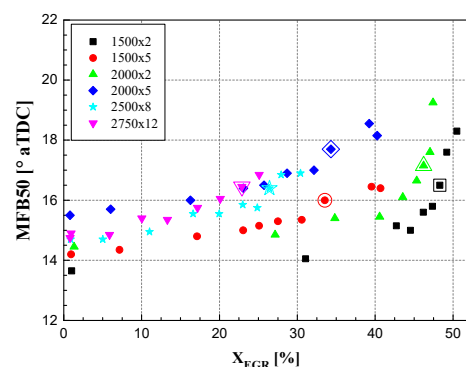


Figure 14. Combustion phasing versus X_{EGR} .

259 When the exhaust gas is recirculated to the cylinder inlet at a low load, the unburned HC in the exhaust gas burn
260 because sufficient O_2 is available in the combustion chamber and the intake temperatures are relatively high. However,
261 $bsfc$ increases with X_{EGR} for heavy EGR rates and $bmeP = 2$ bar, as there is not enough fresh air to burn all the injected
262 fuel, and this represents a drawback for the use of EGR rates beyond $X_{EGR} \approx 40\%$. $bsfc$ is less affected by the EGR rate at
263 medium and high loads. The influence of EGR on the $bsfc$ for $bmeP \geq 5$ bar does not show a definite trend up to
264 $X_{EGR} \approx 20\%$. A small increase in $bsfc$ can be observed for higher EGR mass fractions than 20%, mainly due to the
265 reduction in λ and to the longer duration of combustion.

266 Figure 12 plots the combustion noise (CN) as a function of X_{EGR} . The influence of EGR at $bmeP = 2$ bar and $bmeP = 5$
267 bar, is virtually negligible up to $X_{EGR} \approx 45\%$, whereas an important decrease in CN can be found for $X_{EGR} > 45\%$ at
268 $bmeP = 2$ bar. A continuously decreasing trend can be detected at higher loads, i.e. $bmeP = 8$ bar and $bmeP = 12$ bar, for
269 $X_{EGR} \leq 30\%$.

270 Combustion stability is not affected to any great extent by the EGR rate, since the coefficient of variation of $imeP$
271 (COV_{imeP}) is always lower than 3%, as can be seen in Fig. 13, and no well-defined trend of COV_{imeP} with respect to X_{EGR}
272 can be observed. Fig. 14 plots the crankshaft angle at which 50% of the mixture has already burned, i.e. $MFB50$, as a
273 function of the EGR . The influence on the combustion duration results to be appreciable even for small EGR mass
274 fractions and becomes more evident for higher X_{EGR} than 40%. $MFB50$ is delayed for all the examined key-points, as
275 X_{EGR} is augmented, since EGR slows the chemical reactions.

276 **5. CRANKSHAFT BASED DIAGRAMS FOR THE MAIN IN-CYLINDER QUANTITIES.**

277 Figures 15-24 report the unburned gas mass (M_u), the in-cylinder pressure (p_{cyl}), the HRR , the in-cylinder burned zone
278 gas temperature (T_b), the NO_x and the soot as functions of the crankshaft angle. The p_{cyl} traces were acquired
279 experimentally using 0.1° CA (crank angle degree) steps and were averaged over 100 consecutive engine cycles; the
280 HRR was evaluated by means of a standard 1 zone diagnostic tool on the basis of the p_{cyl} distribution, while the histories
281 of M_u , T_{cyl} , NO_x and soot were calculated by means of a three-zone diagnostic tool on the basis of the p_{cyl} data. The
282 diagnostic model fitting coefficients were calibrated on the basis of the experimental engine-out emissions [42].

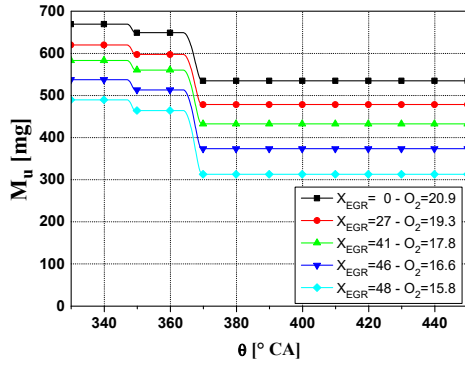


Figure 15. Unburned gas mass as a function of $\theta(2000 \times 2)$.

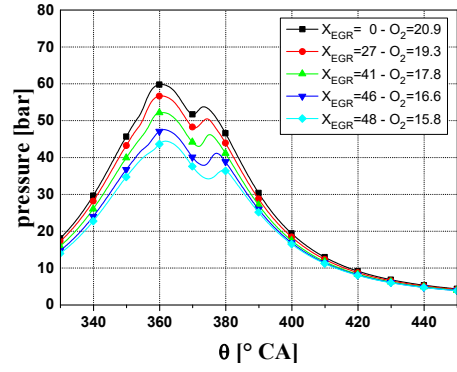


Figure 16. In-cylinder pressure as a function of $\theta(2000 \times 2)$.

283 The unburned mass M_u accounts for the mixture that has not yet burned at the considered crank angle. Before injection
 284 has occurred, M_u is equal to the sum of the inlet fresh air, the EGR and the residual gas mass fraction from the previous
 285 cycle. As injection takes place, some fuel enters the combustion chamber and mixes with the unburned gases and, as a
 286 result, a mixture zone is formed, in which the mass ratio of the air to the fuel is approximately stoichiometric. The
 287 unburned mass progressively reduces during the injection and combustion period, as is shown in Fig. 15 for the 2000×2
 288 key-point, since part of the initial M_u enters the model mixture zone [42]. The increase in the EGR rate makes the value
 289 of M_u at $\theta=330^\circ$ CA decrease, due to a diminution in the inlet charge density (thermal throttling effect). This reduction
 290 in M_u with X_{EGR} determines a reduction in the in-cylinder pressure before combustion, and a more intense reduction

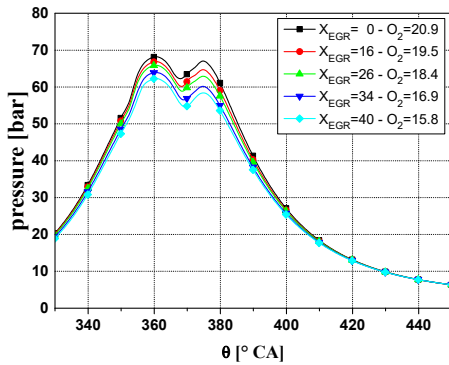


Figure 17. In-cylinder pressure as a function of $\theta(2000 \times 5)$.

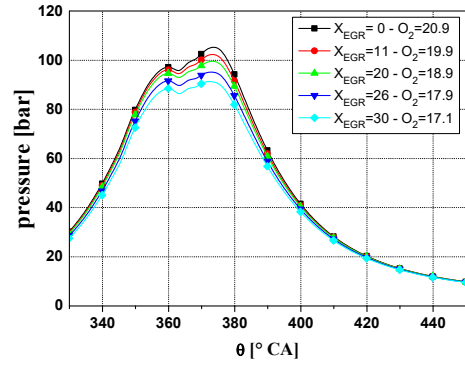


Figure 18. In-cylinder pressure as a function of $\theta(2500 \times 8)$.

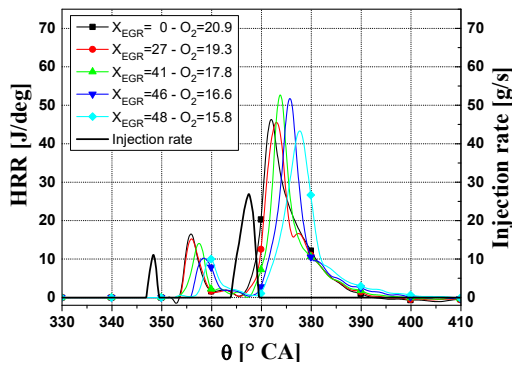


Figure 19. Heat release rate as a function of $\theta(2000 \times 2)$.

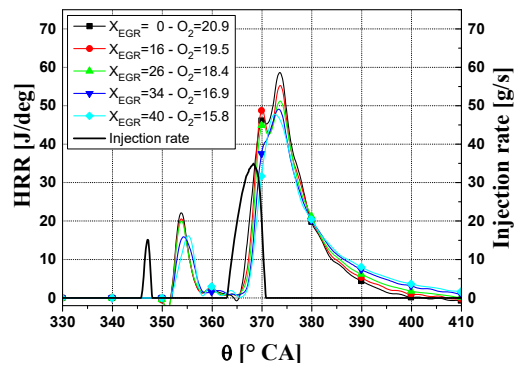


Figure 20. Heat release rate as a function of $\theta(2000 \times 5)$.

291 during both the combustion and the early expansion phases (Fig. 16). Less influence of the EGR on p_{cyl} is detected as
292 the engine load is increased (Figs. 17 and 18), because combustion is more vigorous and the smaller X_{EGR} values induce
293 lower percentage variations of M_u .

294 The HRR (thin lines with symbols) and the injection rate (thick solid line) distributions versus the crankshaft angle have
295 been plotted in Fig. 19 for the 2000×2 key-point. Just one injection rate pattern was plotted in order to avoid the
296 overlapping of many curves, but also considering that the variation with EGR was minor. The first peak in the HRR is
297 related to the pilot injection and is always lower than the second one, which refers to the main combustion. The various
298 changes in the engine inlet charge composition and temperature, due to the EGR rate variations, generally alter the fuel
299 mixing with air and the chemical reaction times, that is, the length of the ignition delay. In particular, the ignition delay,
300 which is evaluated as the distance between the start of injection and the corresponding increase in the HRR of the pilot
301 injection, tends to lengthen in Fig. 19 when X_{EGR} increases, because the dilution effect prevails over the opposing effect
302 of the increase in the temperature of the inlet charge. However, it is also possible that the two opposite effects balance
303 each other, and in these cases, the ignition delay remains almost unchanged with X_{EGR} [23].

304 The combustion mainly occurs in the premixed phase, as can be seen in Fig 19. In fact, when the combustion of the
305 main injected fuel starts, most of the fuel has already been injected and has had enough time to mix with the in-cylinder
306 charge according to a partial $PCCI$ process. Although the increased fuel ignition delay, due to the higher X_{EGR} , leads to
307 an increasing amount of fuel that burns in a premixed combustion phase, the reduction in oxygen availability decreases
308 the rate at which the fuel burns in the premixed phase. The prevailing effect depends on the EGR rate value and on the
309 considered injection shot (pilot or main).

310 In Fig. 19, it can be observed that, the HRR peak always decreases for the pilot injection, whereas the growth in the
311 premixed fraction determines an increased and retarded main combustion HRR peak for X_{EGR} values of up to 40-45%,
312 compared to the working condition without EGR . When X_{EGR} is increased beyond 45%, the effect of the deceleration of
313 the chemical reaction kinetics prevails over the increased ignition delay and the main combustion HRR peak decreases
314 with the EGR rate rise. As soon as the load increases, a larger fraction of the mixture burns in the mixing-controlled
315 combustion phase. Furthermore, the ignition delay has been proved to be less sensitive (Fig. 20) or even insensitive to
316 X_{EGR} (Fig. 21); in fact, the unburned gas temperature increases, the combustion reactions become faster and, therefore,
317 the influence of the $[O_2]_{int}$ concentration on the ignition delay becomes marginal. However, the combustion velocity
318 slows down as the EGR rate increases, and the intensity of the HRR peak that corresponds to the main injection
319 continues to decrease as X_{EGR} rises for medium and high loads.

320 Figure 22 plots the in-cylinder NO volume fraction time history (NO represents most of the NO_x , since NO_2 is minor) for
321 the 2000×2 case. The NO time distribution was calculated using the extended Zeldovich model [41]. The NO_{end}/NO_{start}

322 ratio, where the subscripts *start* and *end* stand for the in-cylinder *NO* volume fraction before the start of combustion
 323 (evaluated at $\theta=330^\circ$ CA) and after the end of combustion (evaluated at $\theta=450^\circ$ CA), respectively, tends to decrease as
 324 X_{EGR} increases. The absolute value of NO_{start} is proportional to the product of the *EGR* mass and the NO_{end}
 325 concentration. When X_{EGR} increases, the *EGR* mass grows, while the fraction of *NO* in this mass, i.e. NO_{end} , decreases.
 326 As a result, the absolute value of NO_{start} first increases with X_{EGR} (e.g. from $X_{EGR} = 0$ to $X_{EGR} = 27\%$ in Fig. 22) and then
 327 decreases with it (e.g. from $X_{EGR} = 41\%$ to $X_{EGR} = 48\%$ in Fig. 22).

328 Figure 23 shows the temperature of the in-cylinder burned gases, which was calculated in the combustion chamber for
 329 different *EGR* mass fractions for the 2000x2 case. The *EGR* reduces the combustion peak temperatures of the burned
 330 gases and is responsible for the massive reduction in the *NO* concentration at the end of combustion (Fig. 22). The
 331 growth in the intake temperature, due to the increase in the *EGR* mass fraction, leads to slightly raised unburned gas
 332 temperatures during the compression phase. This behavior is not in conflict with the decreasing trend of NO_x with X_{EGR} ,
 333 since the NO_x emissions are closely correlated to the peak temperature of the burned gas zone ($T_{bmax,main}$ around $\theta \approx 360^\circ$
 334 CA in Fig. 23) as well as to the residence time of the burned gases at higher temperatures than 1900-2000 K, but not to
 335 the average gas temperatures in the cylinder.

336 The soot formation and the soot oxidation phases are outlined in Figs. 24-26. Different engine soot emission trends,
 337 with respect to X_{EGR} , can be observed on the basis of the considered load. Soot formation depends on the local
 338 temperature and on $[O_2]_{int}$. The dilution effect of *EGR* has a reduced impact on $[O_2]_{int}$ at low loads (Fig. 24), because of
 339 the relatively high value of λ . On the other hand, an increased *EGR* mass determines a significant reduction in the
 340 burned gas temperature and a consequent reduction in both soot formation and oxidation. The former effect prevails
 341 over the latter, and the soot evaluated at $\theta \approx 450^\circ$ CA results to reduce in Fig. 24 when X_{EGR} is increased. In other words,
 342 most of the fuel is burning under a premixed phase at low loads: fuel, fresh air and *EGR* are mixed thoroughly prior to
 343 combustion, local fuel-rich regions are reduced and combustion temperatures are decreased by *EGR*. On the other hand,

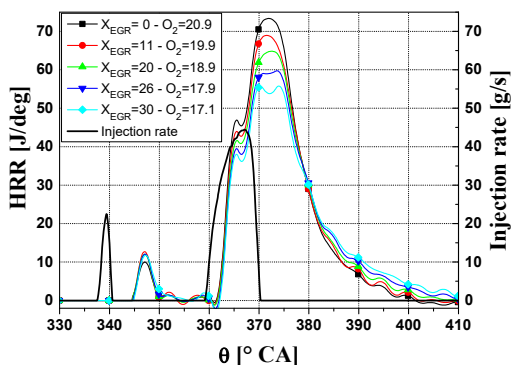


Figure 21. Heat release rate as a function of θ (2500x8).

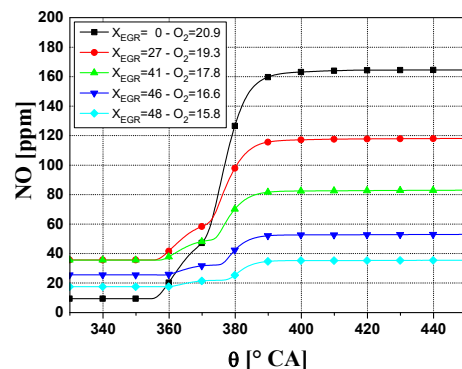


Figure 22. *NO* as a function of θ (2000x2).

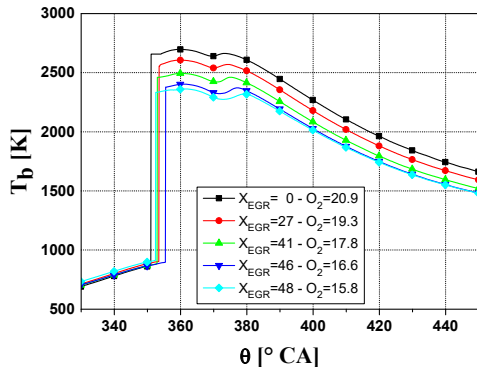


Figure 23. Burned gas temperature as a function of θ (2000x2).

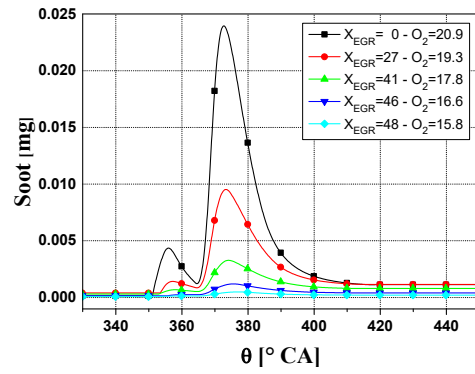


Figure 24. Soot as a function of θ (2000x2).

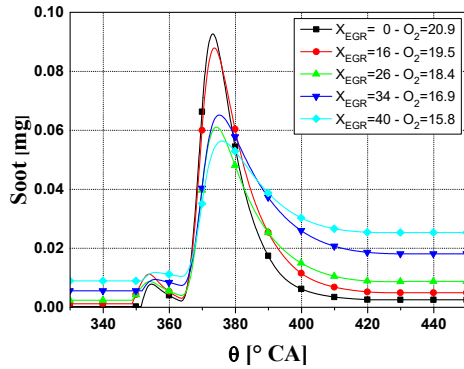


Figure 25. Soot as a function of θ (2000x5).

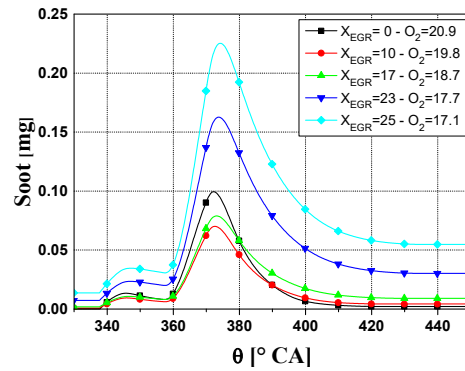


Figure 26. Soot as a function of θ (2750x12).

344 the soot levels observed in Fig. 24 at all the X_{EGR} values are generally not a reason for concern.
 345 The soot formation rate for medium loads ($bmep = 5$ in Fig. 25), continues to reduce as the EGR rate is increased, but
 346 the oxidation rate becomes very low for high EGR rates, because of the reduced in-cylinder temperatures. The latter
 347 effect becomes the prevailing one in determining the fate of soot, which increases with X_{EGR} at the end of combustion.
 348 Finally, at high loads ($bmep = 12$ bar in Fig 26), the augment in X_{EGR} makes λ approach the stoichiometric value, and
 349 this effect prevails over the diminution of the burned gas temperatures, and leads to a significantly increased soot
 350 formation rate. The soot oxidation rate is negatively affected by EGR at high loads, as it is for the low and medium
 351 loads. In short, more soot is measured at the engine exhaust when X_{EGR} grows at high loads.

352 6. CONCLUSIONS.

353 The EGR mass fraction has been varied within the 0÷50% range at different steady-state key-points for an automotive
 354 Euro 5 low compression ratio diesel engine with an optimized pilot-main double injection strategy, managed with a late
 355 $PCCI$ type combustion strategy. The selected key-points are representative of the engine application to a vehicle
 356 running the $NEDC$. The analysis has been performed considering both the time averaged quantities measured at the test
 357 bench and results derived from the application of diagnostic combustion models to the ensemble in-cylinder pressure
 358 time history. Attention has been paid to the benefits that high EGR rates can have on NO_x reduction and to any possible
 359 simultaneous detrimental effects. The largest range of EGR rates has been explored without finding an optimal value for

360 X_{EGR} , which is established as a trade-off between different engine-out emissions and brake specific fuel consumption,
361 but also depends on the synergy between the combustion strategy and the installed aftertreatment devices.

362 The main achievements of the research investigation are synthetically listed hereafter:

363 • The ignition delay tends to increase at low loads as the EGR increases as a result of the reduction in the oxygen
364 concentration because the EGR dilution effect prevails over the increase in the temperature of the inlet charge (thermal
365 throttling effect). The ignition delay has been proved to be less sensitive or even insensitive to X_{EGR} at medium and high
366 loads because the unburned gas temperature increases, the combustion reactions become faster and the influence of the
367 $[O_2]_{int}$ concentration becomes marginal.

368 • The utilization of the EGR generally determines an almost linear decrease in λ when X_{EGR} increases. However, if
369 high EGR rate values, which are typical of PCCI type engines, are applied at low loads, a deviation from linearity
370 occurs, since the desired level of boost pressure that is set by the ECU cannot be maintained in the intake manifold. In
371 fact, the high mass flow-rate, which is sent back from the exhaust to the intake manifold, determines an insufficient
372 enthalpy flux to the turbine. Furthermore, fresh-air throttling reduces the pressure in the intake manifold.

373 • The NO_x emission data, referring to the different key-points, are more closely correlated to $[O_2]_{int}$ than to the
374 maximum burned gas temperature. An almost quadratic monotonically increase in NO_x has been found with respect to
375 $[O_2]_{int}$. The combustion timing of the main injection has also been confirmed to have a significant impact on reducing
376 NO_x emissions. The best results, in terms of NO_x reduction, have therefore been achieved in late PCCI type strategies,
377 when the combustion timing is retarded and high EGR rates are applied.

378 • The HC and CO emissions are relevant at low loads for partial PCCI engines subjected to heavy EGR rates,
379 because fuel over-mixing and wall-quenching occur, due to the very lean mixture and the low temperatures. The
380 influence of EGR on these emissions is not so significant, if EGR rates of up to 30-40% are applied, as occurs in
381 conventional diesel combustion systems, and, in these conditions, EGR can even have a positive effect on HC
382 emissions.

383 • Soot is sensitive to the EGR rate and increases exponentially with the EGR rate at medium and high conditions.
384 The increase in soot with X_{EGR} is mainly due to the lack of oxygen in the recirculated exhaust gases. It is therefore
385 difficult to employ high EGR rates at medium and high loads, due to diffusive combustion deterioration. Therefore, soot
386 and NO_x show a trade-off behavior, with respect to X_{EGR} , at medium and high loads. On the other hand, heavy EGR rates
387 allow NO_x and soot emissions to be improved simultaneously at low loads, because the low compression ratio engine
388 works in partial PCCI mode.

389 • Brake specific fuel consumption is hardly affected by the EGR rate at medium and high loads. The influence of
390 EGR on the $bsfc$ for $bmeP \geq 5$ bar does not show a definite trend up to $X_{EGR} \approx 20\%$. A small increase in $bsfc$ can be

391 observed for higher *EGR* mass fractions than 20%, mainly due to the reduction in λ and to the longer duration of
392 combustion. Instead, a decrease in *bsfc* can be found when passing from no *EGR* to around $X_{EGR} \approx 30\%$ at low loads.
393 This is related to the combustion of the unburned hydrocarbons that enter the combustion chamber with the cooled
394 *EGR*, which involves more O_2 at low loads than at higher loads and acts as a pre-heater of the intake mixture. However,
395 *bsfc* increases with X_{EGR} for heavy *EGR* rates at low loads, due to a lack of fresh air, which is necessary to burn all the
396 injected fuel, and this represents a drawback for the use of high *EGR* rates in *PCCI* strategies.

397 • The stability of the combustion is not affected significantly by the *EGR* rate: the coefficient of variation of the *imep*
398 is always lower than 3% for all the considered *EGR* mass fractions. The increase in the *EGR* rate generally makes the
399 combustion noise decrease, but the effectiveness of this measure depends on the engine load and on the *EGR* rate. An
400 important reduction in *CN* occurs under heavy *EGR* rates for the *PCCI* working mode.

401 7. NOMENCLATURE

| | | |
|-----|---------------------------|--|
| 402 | <i>bme_p</i> | brake mean effective pressure |
| 403 | <i>bsfc</i> | brake specific fuel consumption |
| 404 | <i>CA</i> | crank angle |
| 405 | <i>CN</i> | combustion noise |
| 406 | <i>COV_{imep}</i> | coefficient of variation for the specific torque |
| 407 | $[CO_2]_{amb}$ | volume concentration of CO_2 in the external environment |
| 408 | $[CO_2]_{exh}$ | volume concentration of CO_2 in the engine exhaust |
| 409 | $[CO_2]_{int}$ | volume concentration of CO_2 in the intake manifold |
| 410 | <i>ECU</i> | electronic control unit |
| 411 | <i>EGR</i> | exhaust gas recirculation |
| 412 | <i>HC</i> | unburned hydrocarbons |
| 413 | <i>HCCI</i> | homogeneous charge compression ignition |
| 414 | <i>HRR</i> | heat release rate |
| 415 | <i>imep</i> | indicated mean effective pressure |
| 416 | <i>LTC</i> | low-temperature combustion |
| 417 | \dot{m}_a | fresh air mass flow-rate |
| 418 | \dot{m}_{EGR} | exhaust gas mass flow-rate |
| 419 | M_u | unburned gas mass |

| | | |
|-----|-----------------|---|
| 420 | MFB_{50} | angle at which 50% of the combustion mixture has burned |
| 421 | n | engine speed |
| 422 | NO_{start} | NO emissions before the start of combustion |
| 423 | NO_{end} | NO emissions after the end of combustion |
| 424 | NO_x | nitrogen oxides |
| 425 | $[O_2]_{int}$ | oxygen volume concentration in the intake manifold |
| 426 | p_{int} | pressure in the intake manifold (boost pressure) |
| 427 | p_{cyl} | in-cylinder pressure |
| 428 | $PCCI$ | partial premixed charge compression ignition |
| 429 | PM | particulate matter |
| 430 | q_{pil} | volume of fuel injected in the pilot injection |
| 431 | SOI_{Main} | electrical start of the main injection |
| 432 | SOI_{Pil} | electrical start of the pilot injection |
| 433 | T_b | in-cylinder burned gas temperature |
| 434 | $T_{bmax,main}$ | maximum in-cylinder burned gas temperature |
| 435 | TDC | top dead center |
| 436 | X_{EGR} | mass fraction of exhaust gas recirculation |
| 437 | ϕ | equivalence ratio |
| 438 | λ | relative air-fuel ratio |
| 439 | θ | crankshaft angle |

440 **8. REFERENCES.**

- 441 [1] Zheng M, Reader GT, Hawley JG. Diesel engine exhaust gas recirculation—a review on advanced and novel
442 concepts. *Energy Conversion and Management*, 2004, vol. 45, pp. 883–900.
- 443 [2] Ladommatos N, Abdelhalim SM, Zhao H, Hu Z. Effects of EGR on Heat release in Diesel Combustion. SAE
444 Paper No. 980184.
- 445 [3] Pickett LM and Siebers DL. Non-Sooting Low Flame Temperature Mixing-Controlled DI Diesel Combustion.
446 SAE Paper No. 2004-01-1399
- 447 [4] Lapuerta M, Hernandez JJ, Gimenez F. Evaluation of exhaust gas recirculation as a technique for reducing diesel
448 engine NO_x emissions. *Proc Instn Mech Engrs part D J Autom Engrs*, 2000, vol 214, pp. 85-93.
- 449 [5] Heywood JB. *Internal Combustion Engine Fundamentals*. New York, McGraw-Hill International Editions, 1988.

- 450 [6] Zelenka P, Aufinger H, Reczek W, Catellieri W. Cooled EGR—a key technology for future efficient HD Diesels.
451 SAE Paper No. 980190.
- 452 [7] Kreso AM, Johnson JH, Gratz LD, Bagley ST, Leddy DG. A study of the effects of exhaust gas recirculation on
453 heavy-duty Diesel engine emissions. SAE Paper No. 981422.
- 454 [8] Maiboom A, Tauzia X, Helet J. Experimental study of various effects of exhaust gas recirculation (EGR) on
455 combustion and emissions of an automotive direct injection diesel engine, *Energy*, 2008, vol. 33, pp. 22-34..
- 456 [9] Abd-Alla GH., Using exhaust gas recirculation in internal combustion engines: a review, *Energy Conversion and
457 Management*, 2002, vol. 43, pp. 1027–1042.
- 458 [10] Ladommatos N, Abdelhalim SM, Zhao H, Hu Z. The effects of carbon dioxide in exhaust gas recirculation on
459 diesel engine emissions. *Proc Instn Mech Engrs part D J Autom Engns*, 1998, vol. 212, pp. 25-42.
- 460 [11] Agarwal D., Singh SK., Agarwal AK. Effect of Exhaust Gas Recirculation (EGR) on performance, emissions,
461 deposits and durability of a constant speed compression ignition engine. *Applied Energy*, 2011, vol. 88, pp. 2900–
462 2907.
- 463 [12] Hountalas DT, Mavropoulos GC, Binder KB. Effect of exhaust gas recirculation (EGR) temperature for various
464 EGR rates on heavy duty DI diesel engine performance and emissions. *Energy*, 2008, vol. 33, pp. 272–283.
- 465 [13] Park, Y., and Bae, C., 2014. Experimental study on the effects of high/low pressure EGR proportion in a passenger
466 car diesel engine. *Applied Energy*, 2014, vol.133, pp. 308-316.
- 467 [14] Reader GT, Galinsky G, Potter I, Gustafson RW. Combustion noise levels and frequency spectra in an IDI Diesel
468 engine using modified intake mixtures. *Emerging Energy Technol Trans ASME*, 1995, vol.66, pp. 53–58.
- 469 [15] Kouremenos D. A., Hountalas D. T., Binder K. B., The Effect of EGR on the Performance and Pollutant
470 Emissions of Heavy Duty Diesel Engines using Constant and Variable AFR, SAE Paper No. 2001-01-0198.
- 471 [16] McKinley TL. Modeling Sulfuric Acid Condensation in Diesel Engine EGR Coolers. SAE Paper No. 970636.
- 472 [17] Lim J, Kang B, Park J, Yeom Y, Chung S, Ha J. A Study on Exhaust Characteristics in HSDI Diesel Engine Using
473 EGR Cooler. Proceedings of the KSAE 2004 Fall Conference, pp. 306–312.
- 474 [18] Schubiger R, Bertola A, Boulouchos K. Influence of EGR on Combustion and Exhaust Emissions of Heavy Duty
475 DI-Diesel Engines equipped with Common-Rail Injection Systems. SAE Paper No. 2001-01-3497.
- 476 [19] Dennis AJ., Garrner CP., Taylor DHC. The Effect of EGR on Diesel Engine Wear. SAE Paper No. 1999-01-0839.
- 477 [20] Ishiki K, Oshida S, Takiguchi M. A study of abnormal wear in power cylinder of diesel engine with EGR-wear
478 mechanism of soot contaminated in lubricating oil. SAE Paper No. 2000-01-0925.
- 479 [21] Agarwal AK, Singh SK, Sinha S, Shukla MK. Effect of EGR on the exhaust gas temperature and exhaust opacity
480 in compression ignition engines. *Sadhana* Vol. 29, Part 3, June 2004, pp. 275–284.

- 481 [22] Ladommatos N, Abdelhalim SM, Zhao H, Hu Z. The Dilution, Chemical, and Thermal Effects of Exhaust Gas
482 Recirculation on Diesel Engine Emissions - Part 4: Effects of Carbon Dioxide and Water Vapour. SAE Paper No.
483 971660.
- 484 [23] Jacobs T, Assanis D, Filipi Z. The Impact of Exhaust Gas Recirculation on Performance and Emissions of a
485 Heavy-Duty Diesel Engine. SAE Paper No. 2003-01-1068.
- 486 [24] Wilson RP, Muir EB, Pellicciotti FA. Emissions study of a single-cylinder diesel engine, SAE paper No. 740123.
- 487 [25] Zhu Y, Ricart-Ugaz L, Wu S, Cigler J, El-Beshbeeshy M, Bulicz T, Yan J. Combustion Development of the New
488 International 6.0L V8 Diesel Engine. SAE Paper No 2004-01-1404.
- 489 [26] Nitu B, Singh I, Zhong L, Badreshany K, Henein NA, Bryzik W. Effect of EGR on autoignition, combustion,
490 regulated emissions, and ldehydes in DI diesel engines. SAE paper no. 2002-01-1153.
- 491 [27] Uchida N, Daisho Y, Saito T, Sugano H. Combined Effects of EGR and Supercharging on Diesel Combustion and
492 Emissions. SAE Paper No. 930601.
- 493 [28] Park J, Song S, Lee KS. Numerical investigation of a dual-loop EGR split strategy using a split index and multi-
494 objective Pareto optimization. *Applied Energy*, 2015, vol. 142, pp. 21-32.
- 495 [29] Verschaeren, R., Schaepdryver, W., Serruys, T., Bastiaen, M., Vervaeke, L., Verhelst, S. Experimental study of
496 NO_x reduction on a medium speed heavy duty diesel engine by the application of EGR (exhaust gas recirculation)
497 and Miller timing, *Energy*, 2014, vol. 76, pp. 614-621.
- 498 [30] Yao M, Zheng Z, Liu H. Progress and recent trends in homogeneous charge compression ignition (HCCI) engines.
499 *Progress in Energy and Combustion Science*, 2009, vol. 35, pp. 398-437.
- 500 [31] Saxena S, Bedoya ID. Fundamental phenomena affecting low temperature combustion and HCCI engines, high
501 load limits and strategies for extending these limits. *Progress in Energy and Combustion Science*, 2013, vol. 39,
502 pp. 457-488, <http://dx.doi.org/10.1016/j.pecs.2013.05.002>.
- 503 [32] Fang Q, Fang J, Zhuang J, Huang, A. Influences of pilot injection and exhaust gas recirculation on combustion
504 and emissions in a HCCI-DI combustion engine. *Applied Thermal Engineering*, 2012, vol. 48, pp. 97-104.
- 505 [33] Han D, Ickes AM, Bohac SV, Huang A, Assanis DN. HC and CO emissions of premixed low-temperature
506 combustion fueled by blends of diesel and gasoline. *Fuel*, 2012, 99, pp. 13-19.
- 507 [34] Sethi VP, Salariya KS. Exhaust Analysis and Performance of a Single Cylinder Diesel Engine Run on Dual Fuels.
508 *IE(I) Journal-MC*, vol 85, April 2004.
- 509 [35] L. Cornolti, A. Onorati, T. Cerri, G. Montenegro, F. Piscaglia. 1D simulation of a turbocharged Diesel engine with
510 comparison of short and long EGR route solutions. *Applied Energy*, vol. 111, 2013, pp. 1-15.

- 511 [36] d'Ambrosio S, Ferrari A, Spessa E. Analysis of the Exhaust Gas Recirculation System Performance in Modern
512 Diesel Engines. *Journal of Engineering for Gas Turbines and Power*, 2013, Vol. 135, pp. 0816011-08160113.
- 513 [37] R. Manimaran, R. Thundil Karuppa Raj, CFD Analysis of Combustion and Pollutant Formation Phenomena in a
514 Direct Injection Diesel Engine at Different EGR Conditions, *Procedia Engineering*, 2013, vol. 64, pp. 497-506.
- 515 [38] Lee Y., Huh, K. Y. Analysis of different modes of low temperature combustion by ultra-high EGR and modulated
516 kinetics in a heavy duty diesel engine. *Applied Thermal Engineering*, 2014, vol. 70 (1), pp. 776-787.
- 517 [39] Zheng, Z., Yue, L., Liu, H., Zhu, Y., Zhong, X., Yao, M. Effect of two-stage injection on combustion and
518 emissions under high EGR rate on a diesel engine by fueling blends of diesel/gasoline, diesel/n-butanol,
519 diesel/gasoline/n-butanol and pure diesel. *Energy Conversion and Management*, 2015, vol. 90, pp. 1-11
- 520 [40] d'Ambrosio S, Finesso R, Spessa E. Calculation Of Mass Emissions, Oxygen Mass Fraction And Thermal
521 Capacity Of The Inducted Charge In SI And Diesel Engines From Exhaust And Intake Gas Analysis. *Fuel*, 2011,
522 n. 90, issue 1, pp. 152-166.
- 523 [41] d'Ambrosio S., Finesso R., Fu L., Mittica A. and Spessa E., A control-oriented real-time semi-empirical model for
524 the prediction of NOx emissions in diesel engines. *Applied Energy*, 2014, vol. 130, pp. 265–279.
- 525 [42] Finesso R, Spessa E. A real time zero-dimensional diagnostic model for the calculation of in-cylinder
526 temperatures, HRR and nitrogen oxides in diesel engines. *Energy Convers Manage*, 2014, vol.79, pp. 498–510.
- 527 [43] Liu H, Li S., Zheng Z, Xu J, Yao M. Effects of n-butanol, 2-butanol, and methyl octynoate addition to diesel fuel
528 on combustion and emissions over a wide range of exhaust gas recirculation (EGR) rates. *Applied Energy*, 2013,
529 vol. 112, pp. 246–256
- 530 [44] Zamboni, G., Capobianco, M. Influence of high and low pressure EGR and VGT control on in-cylinder pressure
531 diagrams and rate of heat release in an automotive turbocharged diesel engine. *Applied Thermal Engineering*,
532 2013, vol. 51 (1–2), pp. 586-596.